## SUPPLEMENTARY MATERIALS AND METHODS

### Human sample collection

Primary tumor tissues from 83 patients were subjected to whole-transcriptome sequencing, constituting the FJMUUH bulk RNA-seq cohort for transcriptomic analyses. All patient samples were enrolled using pre-established inclusion and exclusion criteria. For high-resolution cellular characterization, 16 tumor samples were selected for single-cell RNA sequencing (scRNA-seq) and stratified a priori according to immune phenotype into inflamed-type (n = 8) and desert-type (n = 8) tumors. In addition, to preserve the spatial organization of the tumor microenvironment, six representative cases (3 inflamed-type and 3 desert-type) underwent spatial transcriptomic profiling. For protein-level validation and correlative analyses, a tissue microarray (TMA) comprising 67 evaluable gastric cancer (GC) specimens was constructed and analyzed by immunohistochemistry. The study was conducted in strict accordance with the Declaration of Helsinki and was approved by the Institutional Review Board of FJMUUH (approval number: 2022XY034). Written informed consent was obtained from all participants prior to sample collection. Detailed clinicopathological characteristics of the patients are provided in Supplementary Tables S1 and S2.

### Bulk RNA sequencing

Total RNA was extracted using TRIzol reagent (Invitrogen) following the manufacturer's protocol. Library construction and sequencing were performed by Novogene Biotechnology Co., Ltd. using the TruSeq SR Cluster Kit v3 (Illumina, GD-401-3001) on an Illumina HiSeq 4000 platform.

### Single-cell RNA sequencing

Human GC tissues were washed with PBS, cleared of blood and adjacent non-tumor tissue, minced, and enzymatically dissociated into single-cell suspensions. Cells were loaded onto the 10x Genomics Chromium platform, and scRNA-seq libraries were prepared using the Chromium Single Cell 3′ Reagent Kit v3 according to the manufacturer's instructions. Libraries were sequenced on Illumina HiSeq X-10 or NovaSeq 6000 platforms. Raw sequencing data were processed using Cell Ranger v7.0 with alignment to the GRCh38 reference genome.. Downstream analyses, including quality control, normalization, dimensionality reduction, clustering, and cell-type annotation, were performed using Seurat v5.3.0.

**Spatial transcriptomics analysis**

FFPE tumor sections were analyzed using the Visium Spatial Gene Expression platform from 10x Genomics. After tissue permeabilization, spatially barcoded cDNA libraries were generated and sequenced on an Illumina NovaSeq 6000 platform. Data were processed using Space Ranger (v2.0.0) and aligned to the GRCh38 reference genome. Low-quality spots were filtered according to the number of detected genes and total UMI counts.

Downstream analyses were performed in R (v4.5.0), mainly using SpaCET (v1.4.0), Seurat (v5.3.0), GSVA, clusterProfiler, ggplot2, and scatterpie. SpaCET was used to deconvolute spatial transcriptomic data and estimate the relative proportions of different cell types in each spot [1]. Based on SpaCET-derived spatial annotations, spots were classified into tumor, interface, and stroma regions, and tumor-region spots were extracted for subsequent analyses. Tumor-region T-cell infiltration was evaluated by combining the inferred proportions of $CD4^+$ and $CD8^+$ T cells.

Pathway activity analysis was performed using gene sets from the Molecular Signatures Database (MSigDB), including the Hallmark collection and GO biological process gene sets. Gene set files

were imported with clusterProfiler, and spot-level pathway activity scores were calculated using ssGSEA implemented in the GSVA package. Pathways of interest included interferon-gamma response, epithelial-mesenchymal transition, WNT/beta-catenin signaling, and TGF-β signaling. Pathway scores were visualized together with spatial coordinates, and tumor-region pathway scores were further extracted for group comparisons. Differences between groups were assessed using the Wilcoxon rank-sum test, and visualizations were generated using ggplot2 and scatter pie.

**Gene set enrichment analysis**

GSEA was conducted using the *clusterProfiler* package in R. Hallmark and Gene Ontology biological process gene sets were obtained from the MSigDB. Gene sets with false discovery rate (FDR) <0.25 and nominal P <0.05 were considered significantly enriched.

**InferCNV analysis**

Epithelial cells identified from scRNA-seq data were extracted for CNV inference. CNV inference was performed using infercnvpy (v1.6.0) implemented in Python., with T cells serving as the reference normal population. Raw count matrices and annotation files were generated according to established workflows (infercnvpy). Analyses were performed with denoising enabled and a cutoff of 0.1. CNV scores were calculated as the quadratic sum of inferred CNV regions.

**Transgenic mouse model**

*Apc*$^{fl/fl}$ (Cat#: 029275) and *Tp53*$^{fl/fl}$ (Cat#: 008462) mice were purchased from Jackson Laboratories (Bar Harbor, ME, USA). *Tff1-CreERT2* mice were obtained from Cyagen Biosciences Inc. (Santa Clara, CA, USA). *Rasal2*$^{fl/fl}$ (Cat#: NM-CKO-205182) and C57BL/6 wild-type mice were purchased from Cyagen Biosciences Inc. (SuZhou, China). *Apc*$^{fl/fl}$, *Tp53*$^{fl/fl}$ and *Tff1-CreERT2* mice were crossed in-house to generate APTc mice (A: *Apc*$^{fl/fl}$,P: *Tp53*$^{fl/fl}$, and Tc: *Tff1-CreERT2*). *Rasal2*$^{fl/fl}$, *Apc*$^{fl/fl}$, *Tp53*$^{fl/fl}$, and *Tff1-*

*CreERT2* mice were crossed in-house to generate RAPTc mice (R: *Rasal2*$^{fl/fl}$;A: *Apc*$^{fl/fl}$;P: *Tp53*$^{fl/fl}$; and Tc: *Tff1-CreERT2*). All mice were maintained on a C57BL/6 genetic background, housed under specific pathogen-free (SPF) conditions with a 12-h light/dark cycle, and provided standard diet and water ad libitum. Sample sizes were determined based on previous studies, preliminary experiments, and standard practices in the field, with n = 6–8 mice per group. For tumor induction, 8-week-old mice received tamoxifen (100 mg /kg/ day, i.p.) intermittently on days 1, 3, 5, and 7. No blinding was performed for animal experiments during group allocation and outcome assessment. All animal procedures were approved by the Animal Experimentation Ethics Committee of Fujian Medical University (Approval No. 2022-NSFC-0397).

**Subcutaneous allograft and limiting dilution assays**

BALB/c nude mice (6–8 weeks old, sex-matched) were obtained from Shanghai SLAC Laboratory Animal Co., Ltd. (Shanghai, China) and maintained under SPF conditions. For subcutaneous allografts, n = 5 mice per group were randomly assigned to control or RASAL2-knockdown groups; each mouse represented an independent biological replicate. YTN3 cells ($3 \times 10^6$; control or RASAL2 knockdown) were injected subcutaneously into the flanks. Oxaliplatin was administered intraperitoneally (2.0 mg/ kg every 3 days). Tumor volume was calculated as $(L \times W^2)/2$, where L is the length and W is the width. For in vivo limiting dilution assays, n = 6 mice per cell dose were used. Graded numbers of YTN3 cells were injected subcutaneously, and tumor-initiating cell frequency was calculated using Extreme Limiting Dilution Analysis (ELDA; http://bioinf.wehi.edu.au/software/elda/).No blinding was performed for animal experiments during group allocation and outcome assessment.

**Mouse derived allograft（MDA） models**

Tumors from APTc mice were excised, fragmented ($3 \times 3 \times 3$ mm$^3$), mixed with Matrigel (Corning, NY, USA), and transplanted subcutaneously into C57BL/6 mice (6–8 weeks old, sex-matched) under ketamine anesthesia (100 mg/ kg, i.p.). When tumors reached ~150 mm$^3$, mice were treated with anti-PD-1 antibody (10 mg/ kg, i.p., every 3 days) alone. No blinding was performed for animal experiments during group

allocation and outcome assessment.

**Patient-derived organoids（PDOs）**

Human gastric antrum tissues were washed with ice-cold PBS, minced, and digested with collagenase A (2.5 mg/mL; C9891, Sigma-Aldrich, USA) at 37 °C for 30 min. After dissociation, cell suspensions were filtered (70 μm; Corning Life Sciences, USA) and centrifuged at 150 × g for 5 min. Cells were embedded in Cultrex low-growth-factor BME (type 2, Pathclear grade) supplemented with EGF (50 ng/mL), FGF10 (100 ng/mL), Wnt3a (100 ng/mL), Noggin (100 ng/mL), R-spondin-1 (1 μg/mL), B27 (1×), gastrin (10 nmol/L), N-acetylcysteine (1 mmol/L), HEPES (1×), and N2 (1×) (reagents from Sigma-Aldrich, PeproTech, R&D Systems, Gibco, or Vanderbilt University). Fifty microliters of BME-cell suspension was plated per well in 24-well plates (Corning) and overlaid with IntestiCult Organoid Growth Medium (STEMCELL Technologies). Organoids were cultured at 37 °C with 5% $CO_2$, with medium changes twice weekly. Second-generation organoids were infected with control or RASAL2-knockdown lentiviruses overnight and analyzed 7 days later. Organoids were quantified in three random ×100 fields (BZ-X700, Keyence) and processed for immunofluorescence after fixation and embedding. The preparation method and culture conditions of mouse organoids were consistent with those of PDOs.

**Tumor spheroid culture**

AGS or HGC-27 control cells, as well as RASAL2-stable knockdown or overexpression cells, were seeded into ultra-low attachment 6-well plates (Corning, USA) and cultured in serum-free DMEM/F-12 medium supplemented with 20 ng/mL epidermal growth factor (EGF; Thermo Fisher Scientific, USA), 10 ng/mL basic fibroblast growth factor (bFGF), 2% B-27 supplement, and 2 mmol/L L-glutamine (Thermo Fisher Scientific, USA). Cells were maintained at 37 °C in a humidified incubator with 5% $CO_2$ for 10 days. Tumor spheres from five randomly selected fields per well were imaged and quantified using an All-in-One fluorescence microscope (BZ-X700; Keyence Corporation, Atlanta, GA, USA).

**Cell lines, culture, and treatment**

Human GC cell lines AGS, HGC-27, MKN45 and MKN28 were purchased from Cellcook Biotechnology Co., Ltd. (Guangzhou, China) and cultured at 37 °C in a humidified incubator with 5% $CO_2$. AGS, MKN45 and MKN28 cells were maintained in RPMI 1640 medium (Gibco, Carlsbad, CA, USA), whereas HGC-27 cells were cultured in DMEM/F-12 (Gibco). The YTN3 cell line was kindly provided by Prof. Sachiyo Nomura (University of Tokyo, Japan) and cultured in DMEM (D6429, Sigma-Aldrich, USA) supplemented with MITO+ Serum Extender (355006, Thomas Scientific, USA).All media were supplemented with 10% fetal bovine serum (FBS; Pricella Biotechnology, China) and 1% penicillin–streptomycin (Biosharp, Hefei, China). Mycoplasma contamination was routinely monitored using the MycoAlert™ Mycoplasma Detection Kit (LT07-418, Lonza, Switzerland), and all cell lines tested negative throughout the study. Cell lines were authenticated by short tandem repeat (STR) profiling and routinely monitored for morphology and growth characteristics, and used within 15 passages after thawing. Cells were treated with Voglibose (1, 2, or 4 μM), recombinant human TGF-β1 (1 ng/ mL), Vactosertib (1 μM) or Okadaic acid (100nM) for the indicated durations. Reagent details are listed in Supplementary Table 3.

**Plasmid and siRNA transfection**

Transient transfections were performed using Lipofectamine RNAiMAX (Invitrogen, USA) in serum-free DMEM according to the manufacturer's instructions. The pLV-RASAL2 overexpression plasmid was obtained from GeneChem (Shanghai, China). RASAL2 siRNAs were purchased from Dharmacon (Lafayette, CO, USA) and Thermo Fisher Scientific (Waltham, MA, USA). Cells were harvested 48 h after plasmid transfection or 72 h after siRNA transfection for downstream analyses. Detailed information is provided in Supplementary Table 3.

**Generation of stable RASAL2 knockdown cell lines**

Lentiviral shRNAs targeting RASAL2 and control shRNA vectors were purchased from VectorBuilder (Guangzhou, China; https://en.vectorbuilder.com/). YTN3 cells were infected with lentivirus in the presence of polybrene (8 μg /mL; TR-1003, Sigma-Aldrich, USA). Seventy-two hours post-infection, cells

were selected with puromycin for two weeks. Knockdown efficiency was confirmed by western blotting. Target sequences are provided in Supplementary Table 3.

**Drug sensitivity prediction**

Drug sensitivity was predicted using the oncoPredict R package trained on GDSC pharmacogenomic data and applied to TCGA and GEO transcriptomic datasets.

**In *vivo* Lymphocyte Depletion**

For $CD8^+$ T-cell depletion, age- and sex-matched C57BL/6 mice bearing established tumors (~150 $mm^3$) were used, with five mice per group (n = 5); each mouse represented an independent biological replicate. Mice received intraperitoneal injections of anti-mouse CD8α monoclonal antibody (clone 53.6.72, Bio X Cell) at a volume of 50 µL diluted in 200 µL InVivoPure pH 7.0 dilution buffer. Antibody treatments were performed every 72 h for a total duration of 21 days.

**In *vitro* limiting dilution assay**

AGS RASAL2-knockdown cells, HGC-27 RASAL2-overexpression cells, or corresponding controls were plated into U-bottom 96-well plates at limiting dilutions (1, 10, or 100 cells per well). For each cell density and cell type, 32 replicate wells (n = 32) were plated per condition, each representing a biological replicate. After 7 days, wells containing tumor spheres were scored, and stem-cell frequency was calculated using Extreme Limiting Dilution Analysis (ELDA).

**Chemotaxis assay**

Peripheral blood mononuclear cells (PBMCs) were isolated from healthy donors using Ficoll-Paque® PLUS (95021-205, VWR, USA). $CD8^+$ T cells were purified from PBMCs using a $CD8^+$ T Cell Isolation Kit (130-096-495, Miltenyi Biotec, Germany) with LS columns and a MidiMACS™ separator, according to the manufacturer's instructions. Cancer cells were seeded in 6-well plates and subjected to RASAL2 knockdown, RASAL2 overexpression, or IgG control treatment. After 48 h, conditioned media were

collected and added to the lower chambers of Transwell inserts (3.0 μm pore size). Purified $CD8^+$ T cells ($1 \times 10^6$ cells /mL) were placed in the upper chambers, and migrated cells were quantified by flow cytometry. Five independent wells per condition (n = 5) were used as biological replicates. Detailed reagent information is provided in Supplementary Tables 3–4.

**Western blotting**

Cells or snap-frozen tissues were lysed in RIPA buffer (Santa Cruz Biotechnology, Dallas, TX, USA) supplemented with protease and phosphatase inhibitors. Protein concentrations were determined using the Bio-Rad Protein Assay Kit (Bio-Rad Laboratories, Hercules, CA, USA). Equal amounts of protein were separated by SDS–PAGE and transferred to PVDF membranes (EMD Millipore, USA). Membranes were blocked with 5% BSA (Sigma-Aldrich), incubated with primary antibodies at 4 °C overnight, followed by HRP-conjugated secondary antibodies at room temperature for 2 h. Signals were detected using enhanced chemiluminescence and imaged with a ChemiDoc Touch Imaging System (Bio-Rad). Band intensities were quantified using ImageJ software (v1.53, Bethesda, MD, USA). Briefly, images were converted to 8-bit grayscale, regions of interest were defined, and background-subtracted gray values were measured. Protein expression levels were normalized to β-actin. At least three biological replicates were analyzed per group. Full-length uncropped immunoblots are provided in the Source Data file.

**Quantitative reverse-transcriptase PCR (qRT–PCR)**

Total RNA was extracted using TRIzol reagent (Invitrogen, Carlsbad, CA, USA) and quantified with a NanoDrop spectrophotometer (Thermo Scientific, RRID:SCR_025369). cDNA was synthesized using oligo(dT) primers and M-MLV reverse transcriptase (TransGen Biotech, Beijing, China). qRT–PCR was performed on an Applied Biosystems 7500 system using TB Green Premix Ex Taq™ II (RR820A, Takara, Japan). Gene expression was normalized to *HPRT1* (human) or *Hprt1* (mouse) and calculated using the 2^−ΔΔCt method. Primer sequences are listed in Supplementary Table 5.

**Immunohistochemistry (IHC) and immunofluorescence (IF)**

IHC staining was performed using the PV-9000 General Two-step Detection Kit (Zhong Shan-Golden Bridge, Beijing, China), adhering strictly to the manufacturer's protocol. Staining was quantified using the H-score method for RASAL2 or by counting positive cells per high-power field for CD8A, Ki67, TUNEL, and cleaved caspase-3. IHC staining of RASAL2 and CD8 in TMA samples was quantified using the H-score method, calculated as $\Sigma(Pi \times i)$, where Pi represents the percentage of tumor cells at each staining intensity and i denotes the corresponding intensity score (0, no staining; 1, weak; 2, moderate; 3, strong).

For IF staining, sections were incubated with primary antibodies followed by Alexa Fluor–conjugated secondary antibodies (Thermo Fisher Scientific; catalog numbers listed in Supplementary Tables 3–4) and counterstained with DAPI. Images were acquired using a Leica SP5 confocal microscope.

**Chromatin immunoprecipitation (ChIP)**

ChIP assays were performed using ChIP-IT High Sensitivity and ChIP-IT Express Enzymatic kits (Active Motif, Carlsbad, CA, USA). HGC-27 cells were crosslinked with 1% formaldehyde (Sigma-Aldrich) for 10 min at room temperature and quenched with glycine. Chromatin was enzymatically sheared for 12 min and immunoprecipitated overnight at 4 °C with normal rabbit IgG (Millipore Sigma, 3989454), anti-SMAD2/3 (Cell Signaling Technology, 8685T), or anti-BACH1 antibodies (Proteintech, 14018-1-AP). ChIP-enriched DNA was de-crosslinked and analyzed by qRT–PCR. SMAD2/3 occupancy at the BACH1 promoter and BACH1 occupancy at the PD-L1 promoter were quantified, with IgG serving as a negative control. Primer sequences are listed in Supplementary Table 5.

**Co-immunoprecipitation (Co-IP) assay**

Cells were lysed in ice-cold IP buffer (50 mM Tris-Cl, pH 7.4; 150 mM NaCl; 0.5% Triton X-100; 5 mM EDTA) supplemented with protease and phosphatase inhibitors. Lysates were incubated overnight at 4 °C with the indicated antibodies and Protein A/G magnetic beads (Merck Millipore, Billerica, MA, USA). Immunocomplexes were washed, eluted by boiling, separated by SDS–PAGE, and analyzed by western blotting. Antibody details are provided in Supplementary Tables 3–4.

**Dual-luciferase reporter assay**

Luciferase assays were performed using the Dual-Luciferase Reporter Assay System (Promega, E1910). HGC-27 cells were co-transfected with pBACH1/PDL1-Luc or mutant reporters (GeneChem, Shanghai, China) and the pTK-Renilla plasmid. Firefly and Renilla luciferase activities were measured 48 h post-transfection, with Renilla activity used for normalization. Experiments were performed in triplicate.

**Flow cytometry**

Fresh tumor tissues were enzymatically dissociated using type I collagenase A (C9891, Sigma-Aldrich) and filtered to generate single-cell suspensions. Cells were stained with fluorophore-conjugated antibodies at room temperature for 30 min and analyzed on a BD LSRFortessa X-20 flow cytometer (BD Biosciences, Franklin Lakes, NJ, USA). Data were processed using FCS Express v6 software. For in vitro analyses, AGS or HGC-27 cells with RASAL2 knockdown or overexpression were stained with anti-CD44 antibody (Beyotime, ACO112) or IgG control and analyzed by flow cytometry. Five independent biological replicates per condition (n = 5) were analyzed. Antibody details are provided in Supplementary Tables 3–4.

**Immunoprecipitation and mass spectrometry (IP–MS)**

Cells were lysed in ice-cold RIPA buffer supplemented with protease and phosphatase inhibitors. Cell lysates were incubated with an anti-RASAL2 antibody or control IgG at 4 °C overnight, followed by capture with Protein A/G magnetic beads. Immunocomplexes were extensively washed and eluted for subsequent proteomic analysis.

Data-independent acquisition (DIA) raw data were processed and searched using Spectronaut software (version 19). The search parameters were set as follows: peptide length range, 7–52 amino acids; enzyme specificity, trypsin/P; maximum missed cleavages, 2; carbamidomethylation of cysteine as a fixed modification; oxidation of methionine and protein N-terminal acetylation as variable modifications. The false discovery rate (FDR) thresholds were set at $\leqslant$1% at both the protein and peptide levels, with peptide

confidence ⩾99% and an extracted ion chromatogram (XIC) width ⩽75 ppm. Protein quantification was performed using the intensity-based absolute quantification (iBAQ) method. Candidate interactors identified by IP-MS were ranked according to their iBAQ values. After excluding likely nonspecific interactors and focusing on proteins with established roles in phosphorylation-related signaling, PPP1CA emerged as one of the top four candidates.

**Statistical and survival analyses**

Statistical analyses were performed using GraphPad Prism 9.0 (GraphPad Software, USA) and R software v4.1.1 (R Foundation for Statistical Computing, Austria). Data are presented as mean ± SD from at least three independent biological replicates. Normality was assessed prior to analysis. Student's t-test or non-parametric tests were applied for two-group comparisons as appropriate, while multiple groups were analyzed using one-way ANOVA followed by Student–Newman–Keuls or Duncan's post hoc tests. Correlations were evaluated using Pearson's or Spearman's tests. Overall and disease-specific survival were analyzed by the Kaplan–Meier method with log-rank testing. A two-sided $P < 0.05$ was considered statistically significant.

**References**

1 Ru B, Huang J, Zhang Y, Aldape K, Jiang P. Estimation of cell lineages in tumors from spatial transcriptomics data. Nature communications 2023; 14: 568.

## SUPPLEMENTARY FIGURES AND LEGENDS

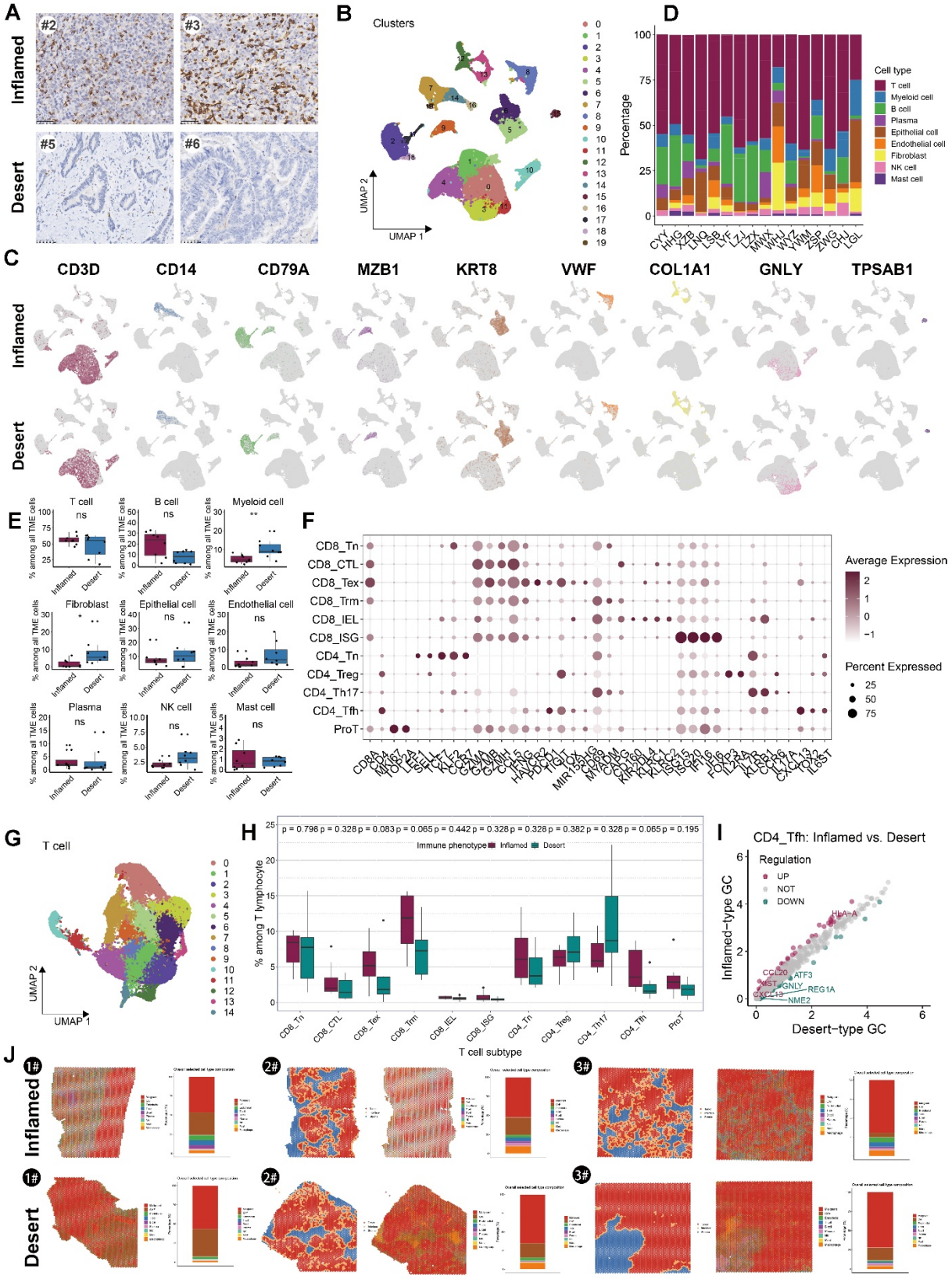

**Fig. S1 Integrated multi-omics analyses at single-cell and spatial resolution delineate inflamed and immune-desert phenotypes in gastric cancer. Related to Fig.1.**

(A) Representative CD8 immunohistochemistry of gastric cancer tissues illustrating dense immune infiltration in inflamed tumors and marked immune exclusion in desert tumors (scale bar, 50 μm). (B) UMAP visualization of 19 clusters in scRNA sequencing data. (C) Marker gene expression characteristics of different cell populations. (D) Stacked bar chart of the proportion of each cell population in tissues from different patients. (E) Changes in the proportion of different cell populations among different immune subtypes. (F) Dot plot illustrating the signature marker gene expression profiles across distinct intratumoral T cell subpopulations. (G) UMAP visualization of T cell subpopulations after re-clustering. (H) Comparative changes in the proportion of T cell subpopulations between inflamed and desert tumor. (I) Differentially expressed genes in CD4_Tfh cells between inflamed and desert tumors. (J) Representative spatial maps from three immune-inflamed (1#–3#, upper panels) and three immune-desert (1#–3#, lower panels) gastric tumors. Left panels show the spatial distribution of major cell populations, middle panels depict tumor (red), interface (orange), and stromal (blue) regions, and right panels show the overall cellular composition of each sample. Statistical analysis: differences between two groups were assessed by Student's t test; Data are presented as mean ± SD. ns, not significant; * $p < 0.05$; ** $p < 0.01$; *** $p < 0.001$; **** $p < 0.0001$.

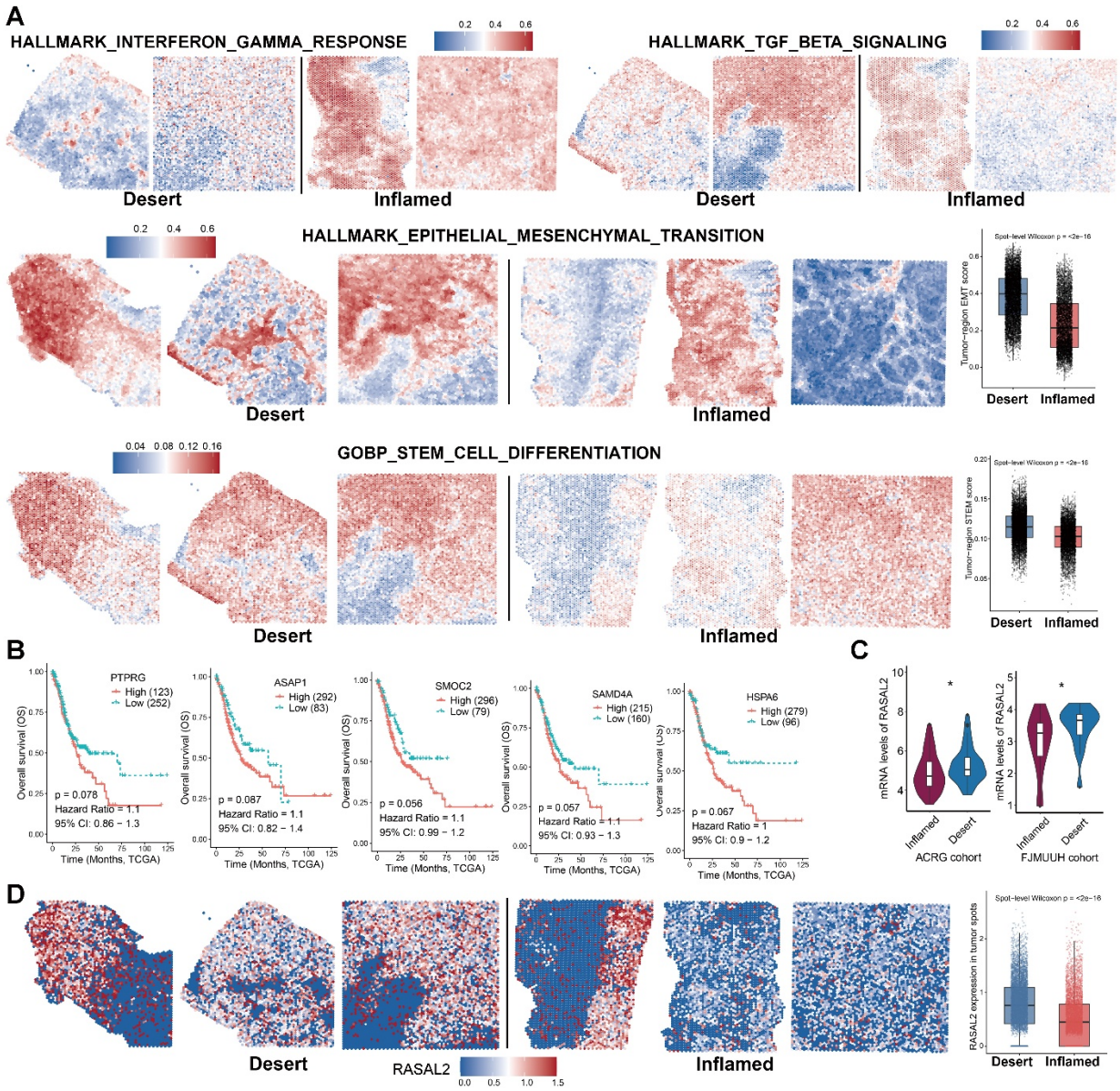


**Fig. S2 Tumor-intrinsic epithelial programs characterize immune-desert gastric cancer. Related to Fig.2.**

(A) Spatial activity maps and quantitative boxplots of IFN-γ response, TGF-β, EMT and stem cell differentiation pathways in desert vs inflamed gastric tumors. (B) Kaplan–Meier overall survival (OS) curves stratified by high/low expression of other five candidate genes (PTPRG, ASAP1, SMOC2, SAMD4A, HSPA6) in the TCGA-STAD cohort; hazard ratios (HR), 95% confidence intervals (CI) and P values are annotated for each gene. (C) Comparison of RASAL2 expression between inflamed and desert tumors in the ACRG and FJMUUH bulk RNA-seq cohorts. (D)

Spatial expression distribution and quantification of RASAL2 in desert and inflamed sections. Statistical analysis: differences between two groups were assessed by Student's t test; Data are presented as mean ± SD. ns, not significant; * $p < 0.05$; ** $p < 0.01$; *** $p < 0.001$; **** $p < 0.0001$.

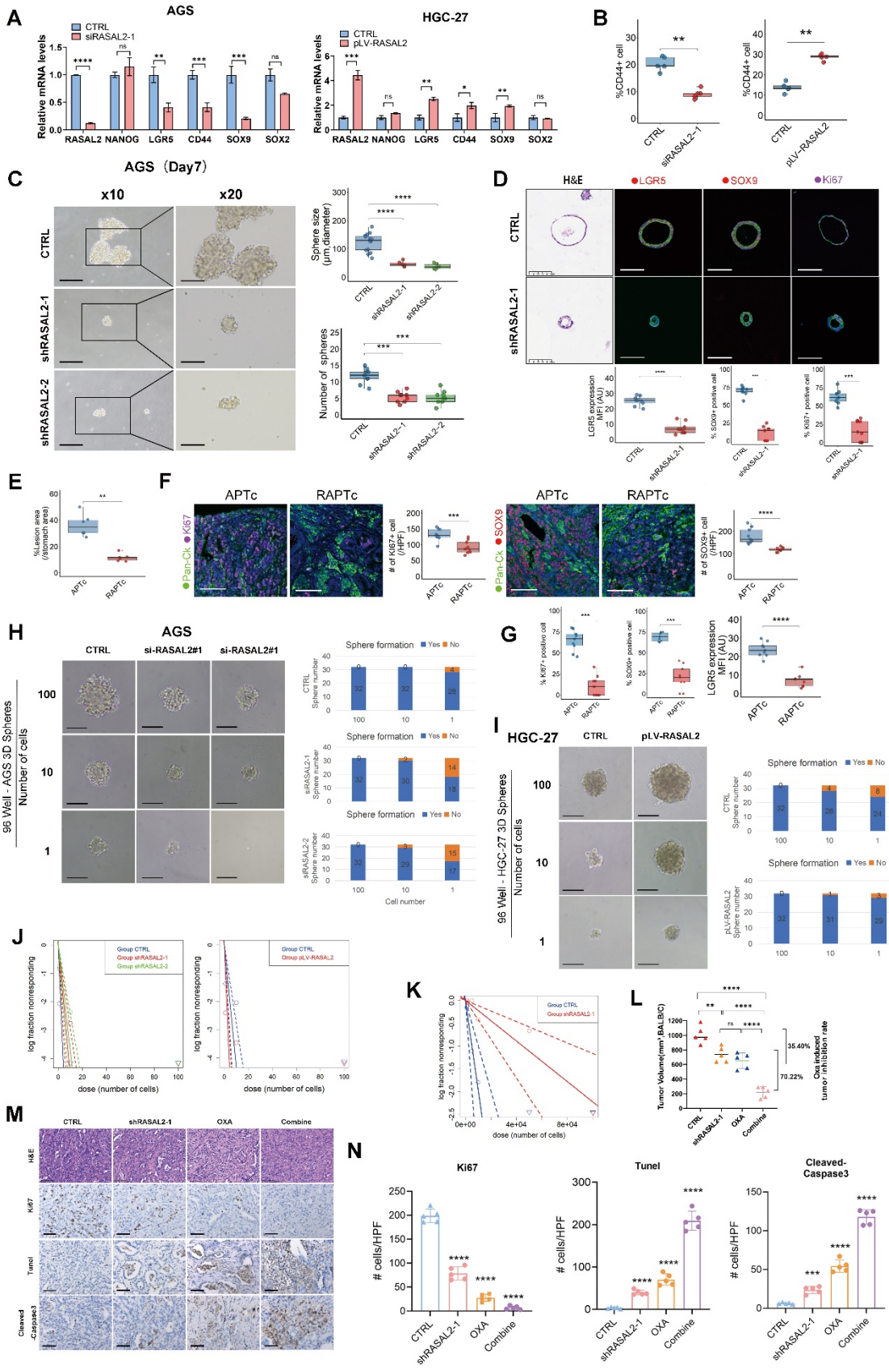
A
AGS
CTRL
siRASAL2-1
Relative mRNA levels
RASAL2 NANOG LGR5 CD44 SOX9 SOX2
HGC-27
CTRL
pLV-RASAL2
B
%CD44+ cell
CTRL
siRASAL2-1
pLV-RASAL2
C
AGS (Day7)
x10
x20
CTRL
shRASAL2-1
shRASAL2-2
Sphere size (μm diameter)
Number of spheres
D
H&E
LGR5
SOX9
Ki67
LGR5 expression MFI (AU)
% SOX9+ positive cell
% Ki67+ positive cell
E
%Lesion area (/stomach area)
APTc
RAPTc
F
Pan-Ck
Ki67
SOX9
# of Ki67+ cell (/HPF)
# of SOX9+ cell (/HPF)
G
H
AGS
si-RASAL2#1
si-RASAL2#2
96 Well - AGS 3D Spheres
Number of cells
Sphere formation
Yes
No
Cell number
I
HGC-27
96 Well - HGC-27 3D Spheres
J
log fraction nonresponding
dose (number of cells)
K
L
Tumor Volume(mm³,BALB/c)
Combine
35.40%
70.22%
M
H&E
Ki67
Tunel
Cleaved-Caspase3
N
Ki67
Tunel
Cleaved-Caspase3
# cells/HPF

**Fig. S3 RASAL2 promotes cancer stemness and tumor-initiating capacity in gastric cancer. Related to Fig.3.**

(A) qRT–PCR analyses of RASAL2 and stemness-associated markers (NANOG, LGR5, CD44, SOX9, SOX2) following RASAL2 knockdown in AGS cells or overexpression in HGC-27 cells. (B) Representative flow cytometry quantification of $CD44^+$ stem-like populations in AGS cells with RASAL2 knockdown or HGC-27 cells with RASAL2 overexpression. (C) Representative images of spheroids derived from AGS cells with stable RASAL2 knockdown (scale bar = 100 μm, left), and quantitative analysis of spheroid size and number (mean ± SD from 3 independent fields, right). (D) Representative immunofluorescence images of Ki67 and stemness markers (SOX9, LGR5) in patient-derived gastric organoids under specific culture conditions (scale bar = 100 μm). (E) Percentage of lesion area relative to total stomach area in APTc and RAPTc mouse models. (F) Immunofluorescence staining of stemness markers (scale bar = 100 μm) and corresponding quantitative analysis in APTc and RAPTc tumor samples; each group included 3 samples, and 9 fields were analyzed per sample. (G) Quantitative analysis of immunofluorescence staining for Ki67 and stemness markers (SOX9, LGR5) in organoids derived from APTc and RAPTc gastric cancer tissues under specific culture conditions. (H–I) Representative bright-field images of 3D spheres (left) and quantitative analysis of sphere-positive and sphere-negative wells (right) for AGS cells transfected with control or si-RASAL2 (H) and HGC-27 cells expressing vector control or pLV-RASAL2 (I), seeded at 100, 10, or 1 cell per well in 96-well plates. (J) Extreme limiting dilution analysis (ELDA) of sphere-forming cell frequency. Left, ELDA plots for control, shRASAL2-1, and shRASAL2-2 AGS cells. Right, ELDA plots for vector control and pLV-RASAL2 HGC-27 cells. The x-axis indicates the number of cells seeded per well, and the y-axis shows the log fraction of non-sphere-forming wells. Dashed lines represent 95% confidence intervals. (K) ELDA-based limiting dilution assay showing tumor-initiating cell frequency in control and shRASAL2-knockdown YTN3 cells. (L) Scatter plot with median lines showing final tumor volumes ($mm^3$) in BALB/c mice bearing control (CTRL), shRASAL2-1, oxaliplatin-treated (OXA), or combined shRASAL2-1 plus oxaliplatin (Combine) xenografts. (M) Representative images of H&E staining and immunostaining for Ki-67, TUNEL, and cleaved caspase-3 in xenograft tumor sections from the CTRL, shRASAL2-1, oxaliplatin (OXA), and shRASAL2-1 + OXA (Combine) groups (scale bar = 50 μm). (N) Quantification of Ki-67-positive, TUNEL-

positive, and cleaved caspase-3-positive cells from five randomly selected high-power fields. Statistical analysis: differences between two groups were assessed by Student's t test; Data are presented as mean ± SD. ns, not significant; * $p < 0.05$; ** $p < 0.01$; *** $p < 0.001$; **** $p < 0.0001$.

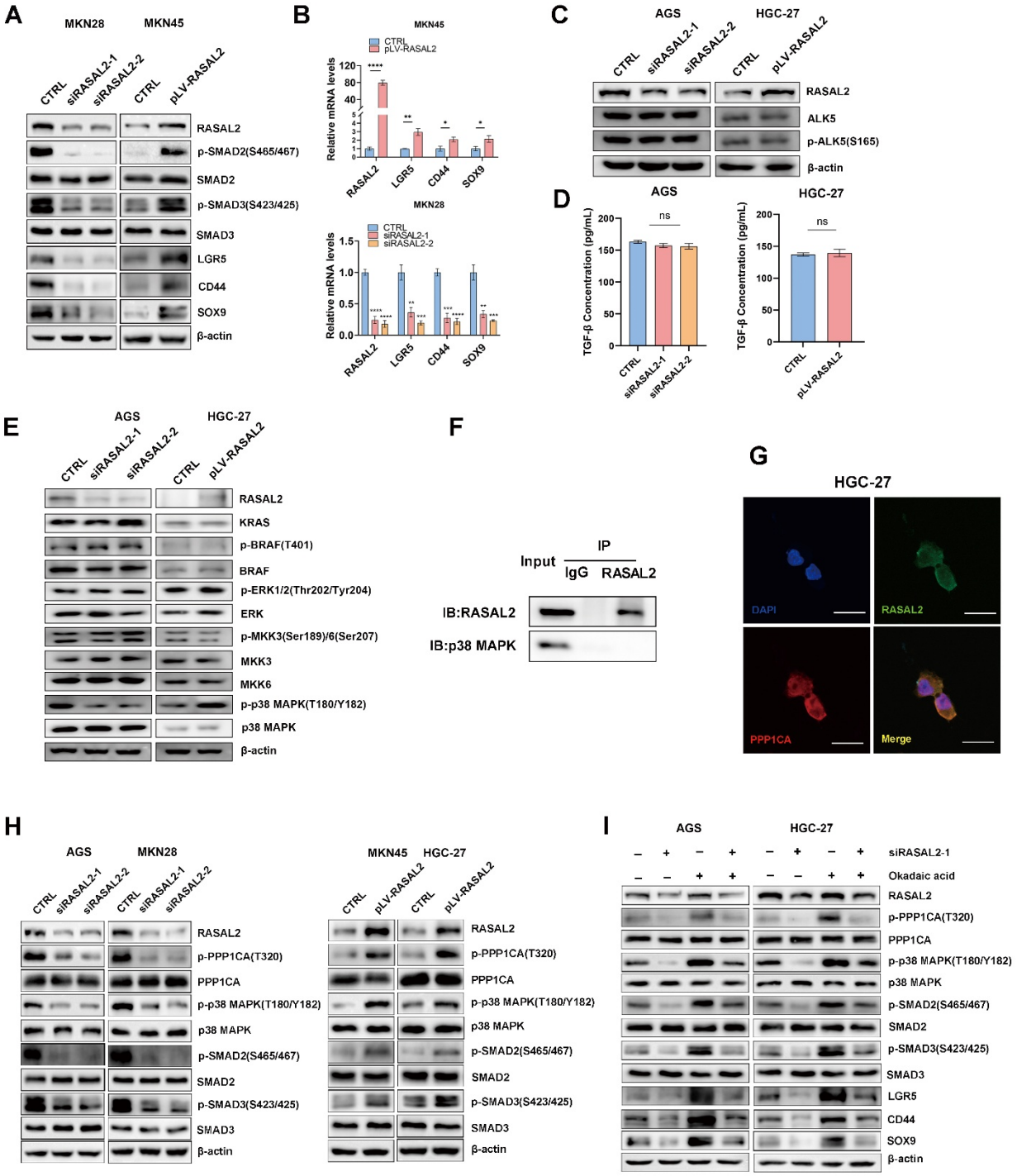

**Fig. S4 RASAL2 sustains cancer stemness through the PPP1CA–p38 MAPK–SMAD2/3 signaling axis. Related to Fig.4.**

(A-B) Immunoblot (A) and qRT–PCR (B) analyses of TGF-β pathway components, and stemness markers following RASAL2 knockdown or overexpression. (C) Western blot analysis of total ALK5 and phosphorylated ALK5 at Ser165 in AGS cells transfected with control or RASAL2-targeting siRNAs and HGC-27 cells expressing vector control or pLV-RASAL2. (D) ELISA analysis of secreted TGF-β levels in the culture supernatants of AGS cells transfected with control or RASAL2-targeting siRNAs and HGC-27 cells expressing vector control or pLV-RASAL2. (E) Western blot analysis of KRAS downstream MAPK signaling in AGS cells with RASAL2 knockdown and HGC-27 cells with RASAL2 overexpression, assessing KRAS, p-/total BRAF, MKK3/6, ERK1/2, and p38 MAPK. (F) Endogenous co-immunoprecipitation analysis of RASAL2 and p38 MAPK in gastric cancer cells. (G) Immunofluorescence colocalization of RASAL2 and PPP1CA in HGC-27 cells (scale bar, 10 μm). (H) Immunoblot analysis of PPP1CA–p38 MAPK–TGF-β/SMAD signaling in gastric cancer cells with RASAL2 knockdown (AGS, MKN28) or overexpression (MKN45, HGC-27). (I) Western blot rescue assay in AGS and HGC-27 cells treated with control siRNA or siRASAL2 ± okadaic acid (OA, 100 nM), assessing PPP1CA–p38 MAPK–TGF-β/SMAD signaling and stemness markers (LGR5, CD44, SOX9). Data are presented as mean ± SD. ns, not significant; * $p < 0.05$; ** $p < 0.01$; *** $p < 0.001$; **** $p < 0.0001$.

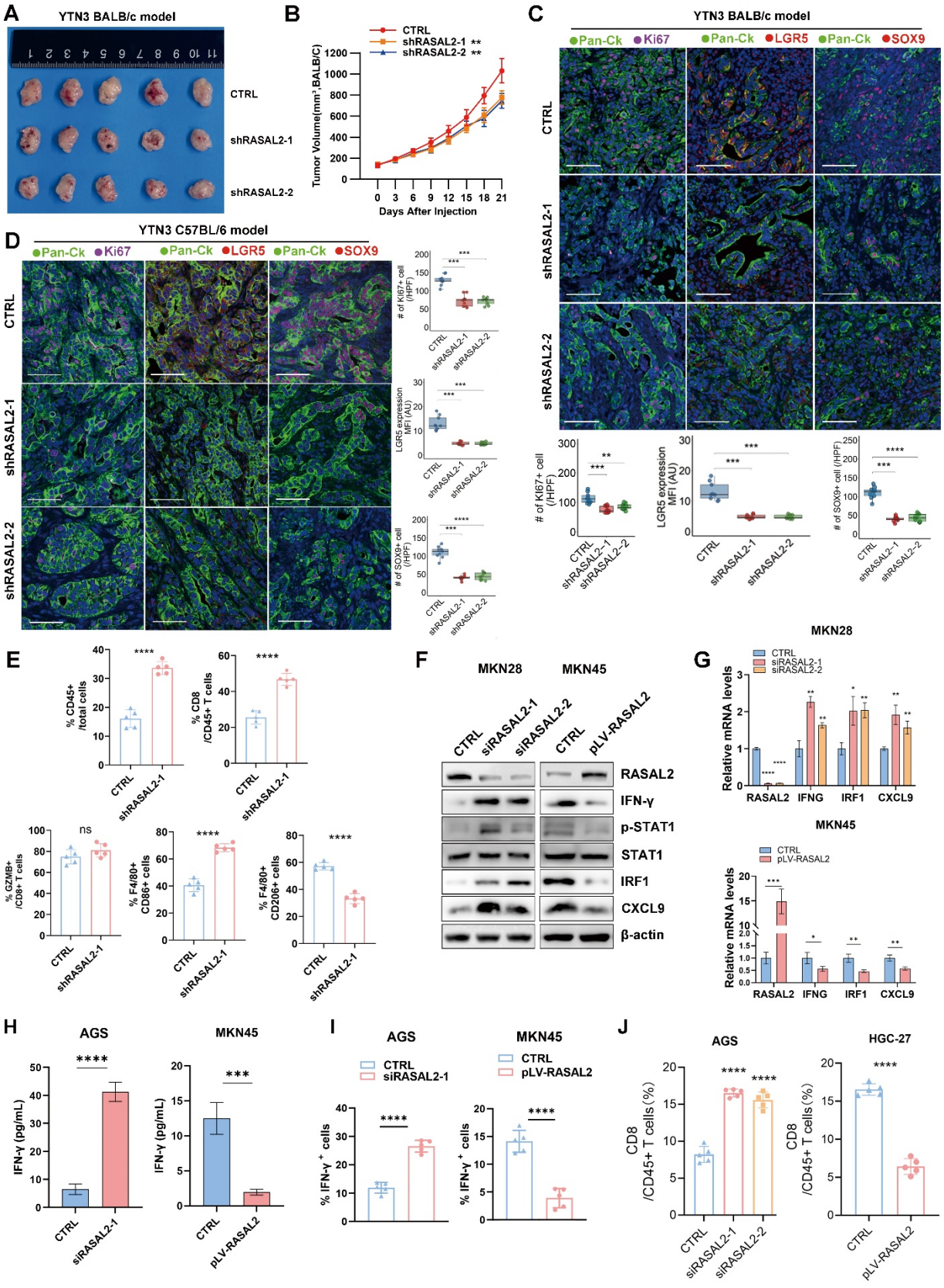
A
YTN3 BALB/c model
CTRL
shRASAL2-1
shRASAL2-2
B
CTRL
shRASAL2-1 **
shRASAL2-2 **
Tumor Volume(mm³,BALB/C)
Days After Injection
C
YTN3 BALB/c model
Pan-Ck Ki67
Pan-Ck LGR5
Pan-Ck SOX9
# of Ki67+ cell (/HPF)
LGR5 expression MFI (AU)
# of SOX9+ cell (/HPF)
D
YTN3 C57BL/6 model
E
% CD45+ /total cells
% CD8 /CD45+ T cells
% GZMB+ /CD8+ T cells
% F4/80+ CD86+ cells
% F4/80+ CD206+ cells
F
MKN28
MKN45
RASAL2
IFN-γ
p-STAT1
STAT1
IRF1
CXCL9
β-actin
G
MKN28
MKN45
Relative mRNA levels
H
AGS
MKN45
IFN-γ (pg/mL)
I
AGS
MKN45
% IFN-γ+ cells
J
AGS
HGC-27
CD8 /CD45+ T cells (%)

**Fig. S5 RASAL2 knockdown promotes CD8$^+$ T-cell recruitment and antitumor immunity via the IFN-γ–STAT1–CXCL9/10 axis. Related to Fig.5.**

(A-B) Representative macroscopic images and growth curves of subcutaneous BALB/C xenografts generated from YTN3 cells with or without stable RASAL2 knockdown (n = 5 per group). (C) Immunofluorescence staining (upper panels; scale bar, 100 μm) and quantification (lower panels) of the proliferation marker Ki67 and stemness markers SOX9 and LGR5 in BALB/c subcutaneous tumors, based on quantification from nine independent microscopic fields per group. MFI, mean fluorescence intensity; HPF, high-power field. (D) Immunofluorescence staining for Pan-CK (tumor epithelium), Ki67, LGR5 and SOX9 in YTN3 C57BL/6 allograft tissues with or without RASAL2 knockdown, accompanied by quantitative statistics (scale bar, 100 μm). (E) Flow cytometric analysis of tumor-infiltrating immune cells in control and shRASAL2 YTN3 xenografts, including CD45$^+$ immune cells, CD8$^+$ T cells, GZMB$^+$ cytotoxic CD8$^+$ T cells, M1 (F4/80$^+$CD86$^+$) and M2 (F4/80$^+$CD206$^+$) macrophages. (F-G) qRT-PCR and immunoblot analyses of the IFN-γ/STAT1/IRF1 pathway following RASAL2 knockdown or overexpression. (H) ELISA measurement of secreted IFN-γ levels in RASAL2-manipulated AGS and MKN45 cells. (I) Flow cytometric analysis of intracellular IFN-γ accumulation in AGS and MKN45 cells following RASAL2 knockdown or overexpression after Brefeldin A treatment. (J) Flow cytometry quantification of CD8$^+$ T cell percentage among CD45$^+$ immune cells after co-culture with RASAL2-knockdown AGS or RASAL2-overexpressing HGC-27 cells. Statistical analysis: differences between two groups were assessed by Student's t test; Data are presented as mean ± SD. ns, not significant; * $p < 0.05$; ** $p < 0.01$; *** $p < 0.001$; **** $p < 0.0001$.

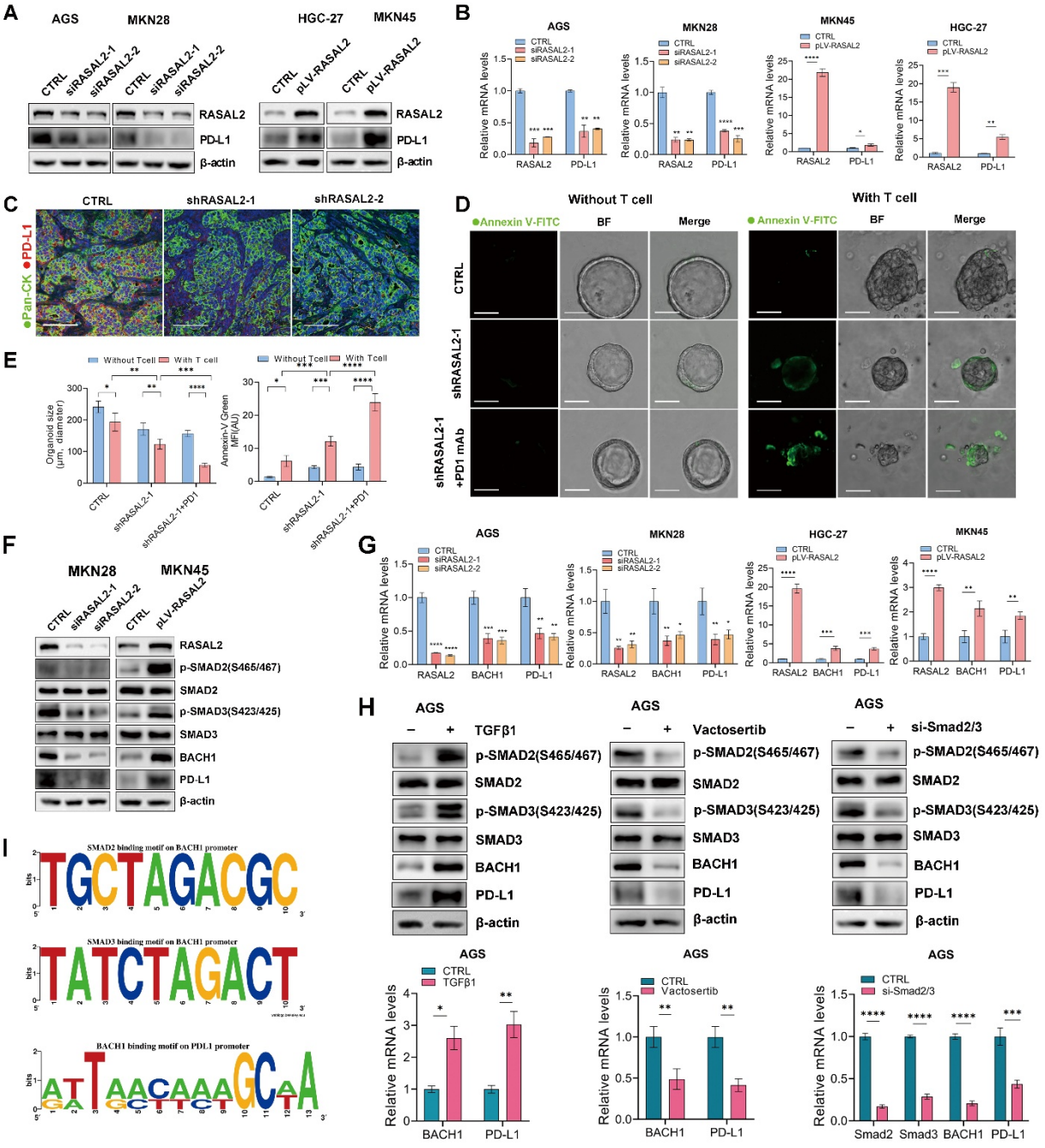


**Fig. S6. RASAL2 enhances PD-L1 expression and immune evasion via SMAD2/3-dependent BACH1 activation. Related to Fig.6.**

(A, B) Western blotting and qRT–PCR analyses of PD-L1 in GC cells with RASAL2 knockdown or overexpression. (C) Immunofluorescence staining (scale bar = 100 μm) to visualize PD-L1 expression in YTN3 BALB/C mouse subcutaneous tumors from control and shRASAL2 knockdown groups. (D, E) Annexin V apoptosis assay in gastric tumor organoid–T cell co-cultures,

with quantitative measurement of organoid diameter and apoptotic Annexin V signal intensity. Three experimental groups (CTRL, shRASAL2-1, shRASAL2-1 + PD-1 neutralizing antibody) were cultured with or without T cells. (F) Immunoblot detection of p-SMAD2/3, total SMAD2/3, BACH1 and PD-L1 in MKN28 (RASAL2 siRNA knockdown) and MKN45 (RASAL2 lentiviral overexpression) cells. (G) qRT–PCR analysis of RASAL2, BACH1, and PD-L1 in GC cells with RASAL2 knockdown or overexpression. (H) Western blotting and qRT–PCR analyses of BACH1 and PD-L1 in AGS gastric cancer cells treated with TGFβ1, the TGFβ receptor inhibitor Vactosertib, or si-Smad2/3 (Smad2/3 small interfering RNA). (I) Promoter binding motif prediction: SMAD2/SMAD3 binding motifs on the BACH1 promoter, and BACH1 binding motif on the PD-L1 promoter (key binding sites marked with distinct colors). Statistical analysis: differences between two groups were assessed by Student's t test; Data are presented as mean ± SD. ns, not significant; * $p < 0.05$; ** $p < 0.01$; *** $p < 0.001$; **** $p < 0.0001$.